Effective Interaction Potentials for Alkali and Alkaline Earth Metal Ions in SPC/E Water and Prediction of Mean Ion Activity Coefficients

Sergei Gavryushov*,† and Per Linse‡

Engelhardt Institute of Molecular Biology, 32 Vavilova St., Moscow, Russia, and Physical Chemistry 1, Center for Chemistry and Chemical Engineering, Lund University, P.O. Box 124, S-221 00 Lund, Sweden

Received: November 27, 2005; In Final Form: February 27, 2006

The potential of mean force (PMF) acting between two simple ions surrounded by SPC/E water have been determined by molecular dynamics (MD) simulations using a spherical cavity approach. Such effective ion−ion potentials were obtained for Me−Me, Me−Cl^-, and Cl^-−Cl^- pairs, where Me is a Li^+, Na^+, K^+, Mg^{2+}, Ca^{2+}, Sr^{2+}, and Ba^{2+} cation. The ionic sizes estimated from the effective potentials are not pairwise additive, a feature in the frequently used primitive model for electrolytes. The effective potentials were used in Monte Carlo (MC) simulations with implicit water to calculate mean ion activity coefficients of LiCl, NaCl, KCl, $MgCl_2$, $CaCl_2$, $SrCl_2$, and $BaCl_2$. Predicted activities were compared with experimental ones in the electrolyte concentration range 0.1−1 M. A qualitative agreement for LiCl and a satisfactory agreement for NaCl were found, whereas the predictions for KCl by two K^+ models were less coherent. In the case of alkaline earth metal ions, all experimental activities were successfully reproduced at $c = 0.1$ M. However, at higher concentrations, similar deviations occurred for all divalent cations, suggesting that the dependence of the permittivity on the salt concentration and the polarization deficiency arising from the ordering of water molecules in the ion hydration shells are important in such systems.

Introduction

Calculations of the potentials of mean force (PMF) acting between ions in electrolyte solution have been a subject of molecular dynamics (MD) and Monte Carlo (MC) simulations for the last two decades. The progress in this area is based on the use of nonpolarizable water models such as the simple point charge model (SPC),[1] the extended simple point charge model (SPC/E),[2] and transferable interacting point sites models (TIPS[3] and TIP4P[4]). These water models were constructed to describe bulk properties[5] and may not adequately describe water near ions. Nevertheless, such water models remain the main tool to study electrolyte solutions due to their simplicity in comparison with models including induced polarizability. The nonpolarizable water models typically have 3−4 fixed charges and a Lennard−Jones (LJ) interaction site centered on the oxygen.

The simplest and the most used representation of ions involves a fixed charge and a LJ interaction site. Today, LJ parameters have been reported for a number of ions, including Li^+, Na^+, K^+, Rb^+, Cs^+, Ag^+, Mg^{2+}, Ca^{2+}, Sr^{2+}, Ba^{2+}, F^-, Cl^-, Br^-, and I^-. The LJ parameters of the ion−water interaction are conventionally obtained by taking means of the LJ parameters for the ion and the water oxygen.

Different experimental properties such as ion hydration energy[6,7] and gas-phase binding enthalpy data for small clusters[8−11] have been used to determine ion−water LJ parameters. Because different types of experimental data are used, several sets of LJ parameters for the same ion−water pair are often available. Preferentially, an experimental verification of other properties than those applied to fit the interaction potential is warranted. For example, the ion LJ potentials of Smith and Dang[8−10] reproduce not only solvation enthalpy, but also the experimental ion−water structural properties. Another issue is that a given ion description developed for a specific water model is transferred to another water model without reparametrization against experimental data.

The potential of mean force acting between ions in an aqueous environment is central for our understanding of electrolyte solution. In the 1980s, an initial step was made by Carnie, Patey, and Kusalik, who applied reference hypernetted-chain approximations for ion−solvent mixtures with water molecules represented by dipole−multipole polarizable hard spheres.[12] Since then, ion−ion PMFs and radial distribution functions (RDF) have been determined from MC and MD simulation studies on electrolyte solutions with explicit water molecules.[13−16] The use of a large number of water molecules, in particular at low ionic concentration, and the need of long simulations (ns range) make such simulations still nontrivial.

An important use of RDFs from atomistic electrolyte simulations is to construct effective ion−ion potentials to be used in coarse-grained simulations without explicit water molecules. For example, Lyubartsev and Laaksonen have presented a method of solving this inverse problem of statistical mechanics.[15] In addition, to study the thermodynamics of diluted electrolyte solutions, this approach has also been used to examine the thermodynamics of macromolecules in electrolyte solutions.[17] The effective ion−ion potentials deduced are dependent on the electrolyte concentration. However, regarding NaCl, its effective potentials demonstrated only a weak salt dependence up to 2 M.[15] Despite its success, the inversion method by Lyubartsev and Laaksonen possesses some accuracy limitations originating from errors in the RDFs and inverse problem solution. More-

* To whom correspondence should be addressed. E-mail: sergei_gavryushov@yahoo.com.
† Engelhardt Institute of Molecular Biology.
‡ Physical Chemistry 1, Center for Chemistry and Chemical Engineering, Lund University.

10.1021/jp056871i CCC: $33.50 © 2006 American Chemical Society
Published on Web 05/12/2006

over, it does not allow determination of effective ion−ion potentials at infinite dilution.

Starting from the pioneering work by Pettitt and Rossky,[18] there have been many attempts of direct computer simulations of the effective ion−ion potentials at infinite dilution, i.e., ion−ion PMFs acting between two isolated ions in water. In some studies, electrically neutral systems were used and the long-range interaction was handled by the Ewald summation,[8,10,19] whereas in other studies, in nonelectroneutral systems, the reaction-field technique was used.[20,21] Moreover, in some simulations, a cutoff of the ion−water and water−water interactions was made,[22] or the Ewald summation was only applied to the water−water interactions.[23] The large selection of boundary conditions and potential truncations demonstrates that not a single technique is optimal. In particular, it is difficult to simulate PMFs of like-charged multivalent ions. To our knowledge, no effective ion−ion potentials at infinite dilution for such ions are yet reported.

In the present work, effective ion−ion potentials between alkali and alkaline earth cations, and a chloride anion in SPC/E water, have been determined from extensive MD simulations. We have employed a spherical cavity, containing two ions and water molecules, surrounded by a dielectric medium, eliminating the complication of the long-range interaction, in particular for systems with a net charge. The effective ion−ion potentials were calculated with high accuracy at a separation between the ions up to 11 Å. Simulations of effective cation−cation, cation−Cl^-, and Cl^-−Cl^- potentials were done with models of Li^+, Na^+, K^+, Mg^{2+}, Ca^{2+}, Sr^{2+}, and Ba^{2+} by Åqvist[6] and of Li^+, Na^+, K^+ Sr^{2+}, and Cl^- by Smith and Dang.[8−11] Throughout, we have employed the rigid SPC/E water model by Berendsen et al.[2]

The effective potentials were used in implicit-solvent MC simulations of electrolyte solutions to calculate ion activity coefficients at electrolyte concentrations between 0.1 and 1 M. Results are compared with experimental activity coefficients. For divalent cations, it was found to be important to include a dependence of the salt concentration on the solution permittivity and a so-called image−cavity interaction term.[24] The latter originates from a polarization deficiency of the ion hydration shell in the field of the second ion. It was approximately introduced in works by Prigogine, Mazur, and Defay,[25] Bolt,[26] Sparnaay,[27] and Levine.[28,29] In the present work, it will be referred to as a polarization deficiency term.

Model and Methods

Two different models are used in this study. First, an atomistic model was employed to calculate the effective interaction, or equivalently, the PMF at infinite dilution, operating between two ions in an aqueous environment. Thereafter, the effective interaction potentials were used to construct solvent-averaged interionic potentials. These potentials were then used in subsequent implicit-solvent simulations to obtain ion activity coefficients.

Atomistic Model Simulations. Two ions and 500 water molecules are enclosed in a spherical cavity of radius R_{RF} surrounded by a dielectric medium with the permittivity ϵ_{RF} representing water (Figure 1). We have employed the SPC/E water potential[2] and different ion potentials representing alkali and alkaline earth metal ions and chloride ion. The LJ parameters (σ and ϵ) of the SPC/E and the polarizable RPOL water model are given in Table 1. Regarding alkali metal ions, simulations were made for Li^+ by using LJ parameters from Åqvist[6] and Dang,[11] Na^+ by using LJ parameters from Åqvist[6] and Dang,[9] and K^+ by using LJ parameters from Åqvist[6] and Dang.[9] As to the alkaline earth metal ions, we have considered Mg^{2+}, Ca^{2+}, Sr^{2+}, and Ba^{2+} by using LJ parameters from Åqvist[6] and Sr^{2+} by using LJ parameters from Smith and Dang.[10] Finally, the LJ parameters for Cl^- were taken from Smith and Dang.[8] All LJ parameters for the ions are compiled in Table 2. It should be noted that the ion models were originally constructed with different water models, viz. the SPC, the SPC/E, or the RPOL model (see Table 2 for details), but will here be used with the SPC/E water model. Any ion polarizability of the original model is here set to zero. Finally, Lorentz−Berthelot mixing rules were used to relate ion−ion, ion−water oxygen, and water oxygen−water oxygen LJ parameters.

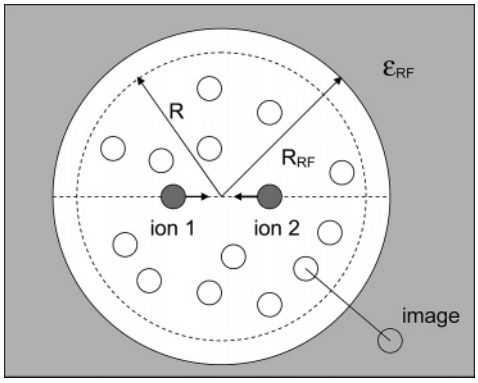

Figure 1. Illustration of the model system composed of a spherical cavity, containing 500 water molecules and two ions at fixed positions, surrounded by a dielectric medium used to simulate the potential of mean forces between the two ions at infinite dilution. $R = 15.3$ Å, $R_{RF} = 18.1$ Å, and $\epsilon_{RF} = \epsilon_{SPC/E} = 71$. See text for further details.

TABLE 1: Lennard−Jones Parameters σ and ϵ for SPC(/E) and RPOL Water[a]

	SPC[b]		RPOL[c]	
atom	σ	ϵ	σ	ϵ
O	3.1655	0.1554	3.196	0.160

[a] Units: σ in Å and ϵ in kcal/mol. [b] Ref 2. [c] Ref 5.

TABLE 2: Lennard−Jones Parameters σ and ϵ for Some Ions[a]

	SPC[b]		SPC/E[c]		SPC/E[d]		RPOL[e]		RPOL[f]	
ion	σ	ϵ	σ	ϵ	σ	ϵ	σ	ϵ	σ	ϵ
Li^+	2.023	0.0183							1.506	0.165
Na^+	3.328	0.00277	2.35	0.130	2.584	0.100				
K^+	4.739	0.000328			3.332	0.100				
Mg^{2+}	1.398	0.875								
Ca^{2+}	2.361	0.45								
Sr^{2+}	3.102	0.118					3.341	0.100		
Ba^{2+}	3.786	0.0471								
Cl^-			4.40	0.100						

[a] Units: σ in Å and ϵ in kcal/mol. [b] Ref 6. Åqvist provides ion−water oxygen LJ parameters, which here have been converted to ion LJ parameters by using the Lorentz−Berthelot mixing rules and LJ parameters of the SPC water model. [c] Ref 8. [d] Ref 9. [e] Ref 10. [f] Ref 11.

The water molecules were initially placed within a spherical volume of radius $R = 15.3$ Å according to experimental water density. Inside the spherical cavity, all interactions were evaluated explicitly. Water molecules interacted with the surrounding via the short-range water−water potential centered at radius $R_{RF} = 18.1$ Å. The leading reaction field of the dielectric medium acting on water molecules and ions was represented by image charges (Figure 1)[30] by using the permittivity of the SPC/E water model, $\epsilon_{SPC/E} = 71$.[31,32] The

equation of motion of the rigid molecules were integrated by using quaternions, and the velocity version of the Verlet algorithm with a time step of 1 fs was used. The simulation times were typical $t_{MD} = 0.9$ or 1.8 ns, in addition to preceding equilibration. The velocities were scaled by using the procedure by Berendsen et al.[33] with a time constant of 0.1 ps. The desired temperature was 298 K, and the averaged temperatures obtained were between 299 and 300 K. All MD simulations were carried out by employing the MOLSIM package.[34]

The mean force operating on an ion was evaluated for fixed positions of the ions (Figure 1). We have used ion−ion separations between 2 Å and 10 or 11 Å with a step of $h = 0.1$ Å, implying 81 or 91 simulations for each mean-force curve. The potential of mean force at ion−ion separation r, $u^0(r)$, was integrated according to

$$u^0(r) \equiv u^0(r_{max}) - \int_{r_{max}}^{r} \frac{1}{2}[F^{(2)}(r') - F^{(1)}(r')]\, dr' \quad (1)$$

by using the trapezoidal rule, with $F^{(1)}(r')$ and $F^{(2)}(r')$ denoting the mean force acting on ion 1 and 2, respectively, at ion−ion separation r' and $u^0(r_{max})$ is the interacting potential at the maximal ion−ion separation. A positive mean force implies a repulsive interaction.

The protocol of these simulations was dictated to achieve effective ion−ion potentials with an accuracy of 0.1 kT over the entire range as examined from separate simulations starting with different initial configurations. As will be further elaborated below, such accuracy of the effective ion−ion potentials is necessary for the determination of ion activity coefficients from implicit-solvent simulations.

The mean forces evaluated using the present setup will be artificially affected when an ion becomes too close to the wall due to the molecular nature of the solvent and, to a lesser extent, of describing distant solvent molecules as a dielectric medium. In separate simulations involving a singe ion and water in a spherical cavity, the mean force acting on the ion was evaluated as a function of its radial position with $\epsilon_{RF} = 1$. Deviations between the simulated mean-force and analytical ion-image force started to appear when the ion−wall separation was ≈10 Å. Despite the fact that the results at this ion−wall separation should be reasonable with $\epsilon_{RF} = 71$, the smallest ion−wall separation in the mean-force simulations was 12.6 Å, occurring for the ion−ion separation of 11 Å.

As mentioned in the Introduction, in the literature, several boundary conditions have been employed to calculate effective ion−ion potentials. The different approaches used to calculate effective potentials have different merits. The present one does not require charge neutrality, which allows us to simulate effective interaction between like-charge ions in a straightforward manner. However, we are only able to obtain effective potentials at infinite dilution.

Solvent-Averaged Interionic Potentials. The effective ion−ion potentials (at infinite dilution) for ions i and j separated by r as obtained from the atomistic simulations $u_{ij}^0(r)$ will now conceptually be divided into two terms. We will use the following division

$$u_{ij}^{\ 0}(r) = u_{ij}^{SR}(r) + u_{ij}^{Coulomb}(r; \epsilon_r), \qquad r \le r_{max} \quad (2)$$

where $u_{ij}^{Coulomb}(r)$ denotes the long-range Coulomb interaction assuming a homogeneous permittivity ϵ_r of the system, and $u_{ij}^{SR}(r)$ is the remaining and short-range part originating from the molecular nature of the solvent. The Coulomb term is given by

$$u_{ij}^{Coulomb}(r; \epsilon_r) = \frac{q_i q_j}{4\pi\epsilon_0\epsilon_r r} \quad (3)$$

In our analysis, the dielectric constant of the SPC/E water model $\epsilon_{SPC/E} = 71$ has been used. Hence, the short-range part $u_{ij}^{SR}(r)$ is evaluated according to

$$u_{ij}^{SR}(r) = u_{ij}^{\ 0}(r) - u_{ij}^{Coulomb}(r; \epsilon_{SPC/E}), \qquad r \le r_{max} \quad (4)$$

where $u_{ij}^0(r)$ is determined from simulations and $u_{ij}^{Coulomb}(r; \epsilon_r)$ is given by eq 3.

Effective ion−ion potentials $u_{ij}(r)$ were used in implicit-solvent MC simulations to calculate ion activity coefficients. The effective potentials were constructed according to

$$u_{ij}(r) = \begin{cases} u_{ij}^{SR}(r) + u_{ij}^{Coulomb}(r; \epsilon_r), & r \le r_{max} \\ u_{ij}^{pol}(r) + u_{ij}^{Coulomb}(r; \epsilon_r), & r > r_{max} \end{cases} \quad (5)$$

where $u_{ij}^{SR}(r)$ is extracted from eq 4 and $u_{ij}^{pol}(r)$ represents a repulsive contribution arising from a polarization deficiency of the ion hydration shell in an external field. The term $u_{ij}^0(r_{max})$ entering in eq 1 was set equal to $u_{ij}^{pol}(r_{max}) + u_{ij}^{Coulomb}(r_{max}; \epsilon_{SPC/E})$, making $u_{ij}(r)$ continuous at $r = r_{max}$.

There are two nontrivial aspects regarding eq 5. The first involves the dielectric constant ϵ_r used in the Coulomb term. We have employed (i) the experimental dielectric constant of water $\epsilon_r = \epsilon_{water} = 78.5$ to correct for the slight difference between the dielectric constant of the SPC/E water model and real water and (ii) a solution permittivity dependent on the electrolyte concentration c according to $\epsilon_r = \epsilon_{solution}(c)$ with

$$\epsilon_{solution}(c) = \epsilon_{water} - \sum_i \delta_i c_i \quad (6)$$

where the sum extends over the ionic species, and δ_i are ion-specific positive-definite factors. The factor δ_i is considerable for a divalent cation, smaller for monovalent cations, and negligible for Cl^-. We have used $\delta_i = 24$, 23, 22, and 20 M^{-1} for Mg^{2+}, Ca^{2+}, Sr^{2+}, and Ba^{2+}, 8 M^{-1} for Na^+, and 2 M^{-1} for Cl^{-1}. These values are close to the experimental data[35−37] and results of simulations.[31] The use of eq 6 approximately corrects for the fact that the effective ion−ion potentials were simulated at infinite dilution but used for finite salt concentrations. The substitution of ϵ_r by the ϵ_{water} relies on the fact that the Coulomb term (eq 3) remains the leading one to very short ion separations.[38]

The second aspect of eq 5 deals with the contribution $u_{ij}^{pol}(r)$ added for distances $r > r_{max}$. For divalent cations, we found that the slope of $u_{ij}(r)$ beyond its oscillatory region deviated from a Coulomb behavior. We attribute this deviation to a dielectric saturation of the ion hydration shell in the presence of the external field from the other ion.[35] In more detail, the electrostatic field of a hydrated ion establishes an orientational order of water molecules near that ion.[39] To the leading order, the free energy cost associated with the reduced dielectric response (a polarization deficiency) of such ordered water molecules near ion i in the electric field E_j emancipating from ion j at separation r can be expressed as[31]

$$u_i^{pol}(r) = \alpha_i E_j^{\ 2}(r) \quad (7)$$

where the ion-specific factor α_i is related to δ_i by the relationship

according to

$$\alpha_i = \frac{1}{1000\, N_A}\frac{\epsilon_0}{2}\delta_i \tag{8}$$

with δ_i being the ion-specific factor also entering in eq 6. Hence, the polarization deficiency correction for ions i and j becomes

$$u_{ij}^{pol}(r) = \alpha_i E_j^2(r) + \alpha_j E_i^2(r) \tag{9}$$

Note, $u_{ij}^{pol}(r)$ is only applied to such ion−ion separations where their hydration shells are not overlapping, i.e., at $r > r_{max} \approx 10$ Å. At shorter distances, we will formally refer all non-Coulombic contribution of the interionic potential to $u_{ij}^{SR}(r)$. Finally, the polarization deficiency potential is treated as pairwise additive, which fundamentally is not correct.

Implicit-Solvent Model Simulations. The calculation of mean ion activity coefficients (excess mean ion chemical potentials) were made for electrolyte concentrations varied from 0.1 to 1 M by using systems containing 216 (1:1 electrolyte) or 324 (2:1 electrolyte) ions in a cubic box and with periodic boundary conditions applied. The long-range Coulomb interaction was handled by using the Ewald summation. When the polarization deficiency term was included, it was truncated at 40 Å.

After equilibration, the production simulations involved 10^4 (1:1 salt) or 4×10^4 (2:1 salt) trial moves per particles at the temperature $T = 298$ K. The ion activity coefficients were calculated by means of the Widom method.[40,41] All MC simulations were performed with the MOLSIM package.[34]

Any error in establishing the zero level of the short-range potential leads to a constant shift of $u_{ij}^0(r)$ and notable errors in the determination of the activity coefficients. Consequently, the far-off tail of the effective ion−ion potential needs to be calculated with high accuracy, even at ion−ion separations where the ion−ion mean force is small. The accuracy of 0.1 kT of the mean force leads to activity coefficients with negligible error for electrolyte concentrations up to 0.1 M and tolerable uncertainties up to 1 M.

Lyubartsev and Laaksonen have discussed the sensitivity of the potential on the activity coefficient at high salt concentration.[16] At 5 M NaCl, they found that an increase of the Na^+-Na^+ potential by only 0.02 kT for ion−ion distances 6−8 Å led to a 10% increase in the activity coefficient. This is in qualitative agreement with our findings.

Results

Monovalent Cations. *Effective Potentials.* We will start to compare the effective Na^+-Cl^- potential obtained for identical water and ion potentials, but using different boundary conditions. This has been done with yet another Na^+ potential[8] by using 0.1-ns-long MD simulations. Figure 2 displays the effective Na^+-Cl^- potential as obtained by (i) using a cubic box with periodic boundary conditions and employing the Ewald summation for the long-range interactions[8] and (ii) the spherical cavity approach (Figure 1). It is observed that the two boundary conditions produce essentially identical effective Na^+-Cl^- potentials. Hence, we conclude that, at least for the present conditions, the two approaches result in very similar effective potentials.

Generally, effective unlike ion−ion potential displays (i) a minimum at ion contact, (ii) a solvent-separated minimum, and (iii) a prominent barrier in between. Sometimes even a weak second solvent-separated minimum appears (Figure 2). Of course, this oscillatory behavior originates from the molecular nature of the solvent. At further separation, the effective ion−ion potential follow closely the Coulomb $1/r$-distance dependence.

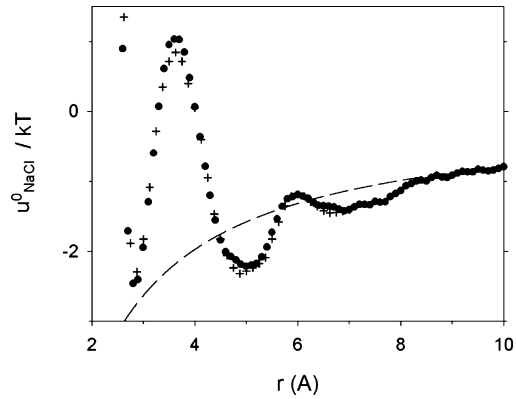

Figure 2. Effective Na^+-Cl^- potentials obtained from MD simulations by using the SPC/E water and ion LJ parameters from ref 8 and employing (i) a cubic box with periodic boundary conditions and the Ewald summation from ref 8 (crosses) and (ii) the spherical cavity approach according to Figure 1 with $t_{MD} = 0.1$ ns (circles). The upper end of the former effective potential was vertically shifted to agree with the later one at $r = 7$ Å. The Coulomb interaction $u_{NaCl}^{Coulomb}(r; \epsilon_r = 71)$ is also shown (dashed curve).

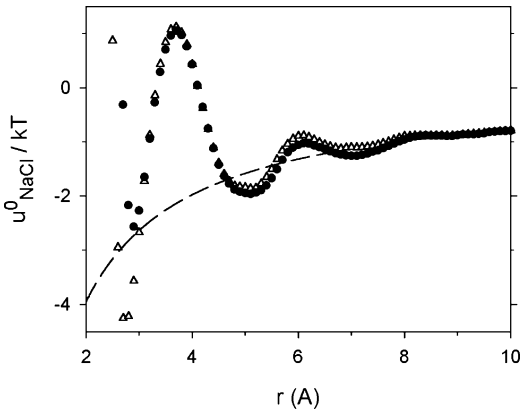

Figure 3. Effective Na^+-Cl^- potentials obtained from MD simulations by using the SPC/E water and Cl^- LJ parameters from ref 8 and Na^+ LJ parameters from ref 6 (triangles) and ref 9 (circles). The Coulomb interaction $u_{NaCl}^{Coulomb}(r; \epsilon_r = 71)$ is also shown (dashed curve). $t_{MD} = 0.9$ ns.

We continue by comparing effective Na^+-Cl^- potentials obtained by using same water and Cl^- models, but different Na^+ models. Figure 3 shows effective Na^+-Cl^- potentials, as obtained with Na^+ LJ parameters from Åqvist[6] and from Dang[9] by using $t_{MD} = 0.9$ ns. The deviations between the two effective potentials are mainly located to the first minimum, which appears at smaller separation (0.2 Å difference) and is deeper (2 kT difference) for Åqvist's Na^+ parameters. We will now argue that this discrepancy is driven by the differences of the two Na^+-Cl^- LJ potentials. The combination of the larger $\sigma_{Na,Cl}$ and the smaller $\epsilon_{Na,Cl}$ appearing in Åqvist's Na^+ model, as compared to those arising from Dang's Na^+ model, leads to a softer LJ repulsion, where the two Na^+-Cl^- LJ potentials cross at $r = 3.2$ Å with $U_{LJ}(r = 3.2\ Å)/kT = 0.2$. At the close-contact minimum separation, the two LJ potentials are shifted by ≈0.15 Å, consistent with our observation. Moreover, such a difference of the close-contact minimum separation implies a more negative direct Coulomb interaction at the shorter minimum separation by ≈10 kT. Obviously, the screening by the water reduces that difference to the observed 2 kT.

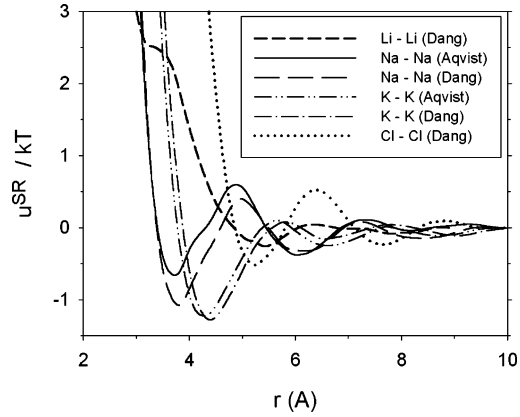

Figure 4. Short-range parts of effective alkali ion−alkali ion potentials from MD simulations by using SPC/E water with Li^+ LJ parameters from ref 11 (short-dashed curve), Na^+ LJ parameters from ref 6 (solid curve) and ref 9 (dash−dotted curve), and K^+ LJ parameters from ref 6 (dash−double-dotted curve) and from ref 9 (short-dashed curve). $t_{MD} = 0.9$ ns. In addition, the short-range part of the effective Cl^-−Cl^- with Cl^- LJ parameters from ref 8 is also shown (dotted curve). $t_{MD} = 1.8$ ns.

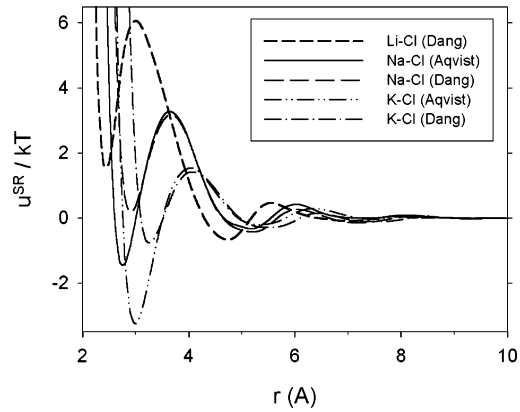

Figure 5. Short-range part of effective alkali ion−chloride ion potentials from MD simulations by using SPC/E water and Cl^- LJ parameters from ref 8. Notation according to Figure 4. $t_{MD} = 0.9$ ns.

Figure 3 also illustrates the small statistical uncertainties of the effective ion−ion potentials from the 0.9-ns-long MD simulations. In the following, we present only spline interpolations of the obtained effective ion−ion potentials.

Short-range parts $u_{ij}^{SR}(r)$ of effective Me^+−Me^+, $Me^+ = (Li^+, Na^+, K^+)$, potentials are given in Figure 4, and the corresponding effective Me^+−Cl^- potentials are displayed in Figure 5. The effective Cl^-−Cl^- potential is also included in Figure 4. Our effective ion−ion potentials are generally in a good agreement with previous results on effective Na^+−Na^+ and Cl^-−Cl^- potentials,[23] on effective Na^+−Na^+, Na^+−Cl^-, and Cl^-−Cl^- potentials,[15,16] and on effective Li^+−Li^+, Na^+−Na^+, K^+−K^+, Na^+−Cl^-, K^+−Cl^-, and Cl^-−Cl^- potentials.[17] In the following, we will first compare the potentials among the different ions and then examine potentials for the same ions but different sources. Because the predictions of the two Li^+ models are close, results from only one of them will be given.

Figure 4 displays that the location of the solvent-separated minima of the short-range effective potentials appearing at $r \approx 6.7$, 6.0, and 5.4 Å decreases in the series K^+, Na^+, and Li^+, as anticipated from the decreasing values of σ_{Me} (Table 2). Similarly, the location of the close-contact minima appearing $r \approx 4.3$ and 3.8 Å decreases in the series K^+ and Na^+. However, regarding Li^+, the close-contact minimum is replaced by an inflection point at ≈3.4 Å, attributed to the strong coordination of the water molecules in the first hydration shell of Li^+, which in turn originates from the small Li^+ size. The principal shape of the short-range Cl^-−Cl^- potential is the same as for the two larger alkali ions; however, the features are displaced to larger separation because of the larger Cl^- size.

The short-range parts of the effective Me^+−Cl^- potentials given in Figure 5 display similar behavior. The location of the solvent-separated and the close-contact minima decreases in the series K^+, Na^+, and Li^+. Moreover, the potential at the close-contact minimum is around zero or negative for Na^+−Cl^- and K^+−Cl^-, but positive for Li^+−Cl^-. The different Li^+ behavior is again consistent with stronger water coordination.

From Figure 5, we notice near the close-contact minimum a similar discrepancy between the two $u_{KCl}^0(r)$ potentials as between the two $u_{NaCl}^0(r)$. As for Na^+, $\sigma_{K,K}$(ref 6) > $\sigma_{K,K}$(ref 9) and $\epsilon_{K,K}$(ref 6) ≪ $\epsilon_{K,K}$(ref 9), implying a similar origin of the discrepancies for the two alkali ion−chloride ion pairs. Finally, Figure 4 shows that the effective alkali ion−alkali ion potentials are less sensitive on the LJ parameters. For example, $u_{KK}^0(r)$ using Åqvist's and Dang's K^+ models are nearly the same, despite the large difference in the corresponding $u_{KCl}^0(r)$ at short separation. Because of the Coulomb repulsion between the two alkali ions, their direct LJ interaction is of marginal importance. The observed differences in $u_{KK}^0(r)$ are instead likely a consequence of the unequal alkali ion−water interactions.

Mean Ion Activity Coefficients. The effective potentials $u_{ij}(r)$ given by eq 5 with the short-range potential $u_{ij}^{SR}(r)$ reported in Figures 4 and 5 were used in solvent-averaged MC simulations to determine mean ion activity coefficients of aqueous LiCl, NaCl, and KCl solutions at concentrations between 0.1 and 1 M.

The role of (i) the permittivity being dependent on the salt concentration and (ii) the polarization deficiency contribution at $r > r_{max}$ was examined by considering the three cases: (A) $\epsilon_r = \epsilon_{water}$ and $u_{ij}^{pol}(r) = 0$; (C) $\epsilon_r = \epsilon_{solution}(c)$ and $u_{ij}^{pol}(r) = 0$; and (D) $\epsilon_r = \epsilon_{solution}(c)$ and $u_{ij}^{pol}(r) \neq 0$ for NaCl solution with Dang's Na^+ potential. Almost identical ln $\gamma_\pm$ was obtained in cases A and D and somewhat smaller ln $\gamma_\pm$ (−0.1 at $c = 1$ M and much smaller deviation at lower salt concentration) for case C. Hence, these two contributions were considered as negligible, and, in the following, case A will be used throughout for the 1:1 electrolytes. The statistical uncertainty in ln $\gamma_\pm$ was estimated to at most 0.01 at $c = 0.1$ M and 0.05 at $c = 1$ M by performing separate atomistic simulations of effective ion−ion potentials for the KCl and NaCl electrolytes with $t_{MD} = 0.9$ ns.

Calculated activity coefficients and corresponding experimental ones are shown in Figure 6. Qualitatively, the predicted activity coefficients follow the experimental trend. In particular, the model simulations reproduce (i) the order $\gamma_{KCl} < \gamma_{NaCl} < \gamma_{LiCl}$ and (ii) an initial decay of γ and a subsequent upturn for LiCl at increasing salt concentration for the salt conditions studied.

Best agreement was obtained for the aqueous solution of NaCl, where experimental[42] γ_{NaCl} is close to those predicted with effective potentials obtained from both Åqvist's[6] and Dang's[9] Na^+ models. The predicted γ_{NaCl} agree with the experiment one up salt concentration $c = 1$ M, which supports the earlier conclusion that three-particle interactions may be neglected at such salt concentrations.[15] The predicted γ_{LiCl} and the predicted γ_{KCl} using Dang's K^+ model agree reasonably with the experimental data, but are systematically too small. The predicted γ_{KCl} using Åqvist's K^+ model is far too small. We relate the much larger underestimation of γ_{KCl} by Åqvist's

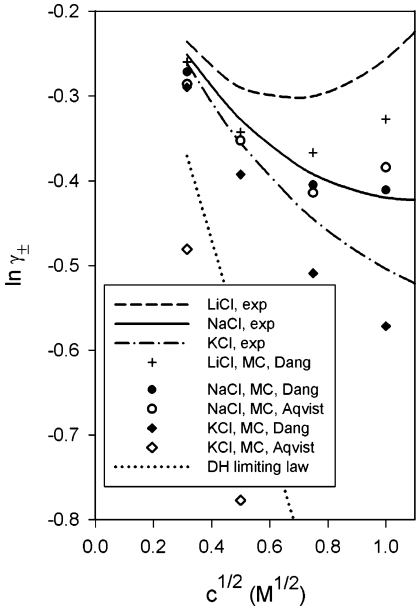

Figure 6. Mean ion activity coefficients vs salt concentration for aqueous solution of alkali metal chlorides from experiments (curves) and MC simulations (symbols). Notation: LiCl (dashed curve and crosses), NaCl (solid curves and circles), and KCl (dashed−dotted curve and diamonds). In the case of NaCl and KCl, alkali ion LJ potential from ref 6 (open symbols) and ref 9 (filled symbols). Equation 5 with $\epsilon_r = \epsilon_{water}$ and $u_{ij}^{pol}(r) = 0$ was used to obtain the effective ion−ion potentials. The Debye−Huckel limiting law is also shown (dotted line).

K^+ model to the more prominent close-contact minimum of the effective K^+-Cl^- potential earlier discussed and shown in Figure 5.

Lyubartsev and Laaksonen[16] have also determined the activity coefficients for aqueous solution of NaCl, but employed effective ion potentials from atomistic simulations at finite ion concentrations by using a cubic cell. They also used Dang's ion potentials, but the flexible SPC water model[43] instead of the SPC/E, the former having a dielectric constant closer to real water. Despite the different protocol and water potentials, very similar ion activity coefficients were obtained. For example, at $c = 0.1$ M, we have $\gamma_{NaCl} = 0.78$ (experimental value), 0.77 (ref 16), and 0.76 (this work). Without the replacement of the permittivity of the SPC/E water with that of real water, we obtained $\gamma_{NaCl} = 0.73$ ($c = 0.1$ M).

Divalent Cations. *Effective Potentials.* As for monovalent cations, we start to compare an effective potential obtained by using two different boundary conditions. Figure 7 displays two effective $Sr^{2+}-Cl^-$ potentials obtained with the same ionic LJ parameters from simulations using (i) the RPOL water model with $\epsilon_r = \epsilon_{RPOL} = 106$, a cubic box with periodic boundary conditions, and the Ewald summation for the long-range interactions[10] and (ii) the SPC/E water model with $\epsilon_r = \epsilon_{SPC/E} = 71$ and our spherical cavity approach with a dielectric medium surrounding the cavity. The comparison of the two approaches is here somewhat hampered by the different water potentials. Nevertheless, good agreement of the locations and magnitudes of the close-contact and solvent-separated minima as well as of the intervening barrier are achieved, again supporting the similarity of the predictions of the two boundary conditions.

Figure 8 shows the simulated effective $Ca^{2+}-Ca^{2+}$ potential $u_{CaCa}^0(r)$, the Coulomb contribution $u_{CaCa}^{Coulomb}(r; \epsilon_{SPC/E})$, and the Coulomb plus polarization deficiency contributions $u_{CaCa}^{Coulomb}(r; \epsilon_{SPC/E}) + u_{CaCa}^{pol}(r)$. It is seen that the slope of $u_{CaCa}^0(r)$ agrees well with the slope of $u_{CaCa}^{Coulomb}(r; \epsilon_{SPC/E}) + u_{CaCa}^{pol}(r)$ between r = 8 and 10 Å, but less satisfactorily with the slope of $u_{CaCa}^{Coulomb}(r; \epsilon_{SPC/E})$. This supports our notion that a repulsive polarization deficiency force appears in the distance regime, where the oscillative short-range force has ceased and before the effective force becomes Coulombic.

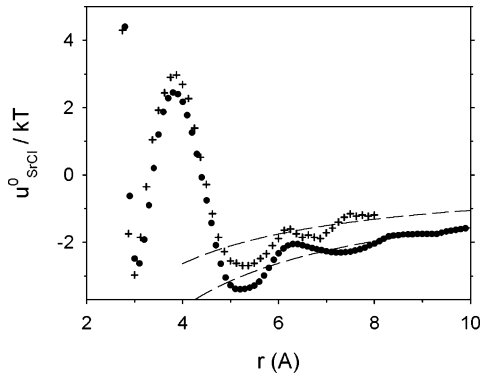

Figure 7. Effective $Sr^{2+}-Cl^-$ potentials obtained by MD simulations by using the Sr^{2+} LJ parameter from ref 10 and Cl^- parameters from ref 8 and employing (i) the RPOL water, a cubic box with periodic boundary conditions, and the Ewald summation from ref 10 (crosses) and (ii) the SPC/E water and a spherical cavity according to Figure 1 with $t_{MD} = 0.9$ ns (circles). The Coulomb interaction $u_{SrCl}^{Coulomb}(r; \epsilon_r)$ with $\epsilon_r = 71$ (lower dashed curve) and $\epsilon_r = 106$ (upper dashed curve) are also shown. The results from ref 10 were obtained in the presence of the second Cl^- ion moving freely inside the box.

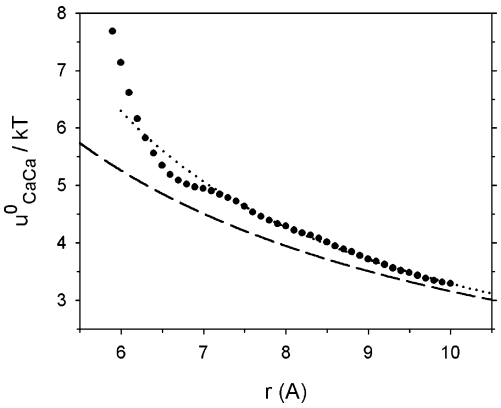

Figure 8. Effective $Ca^{2+}-Ca^{2+}$ potentials obtained by MD simulations by using the SPC/E water, Cl^- LJ parameters from ref 8, and Ca^{2+} LJ parameters from ref 6 (circles). $t_{MD} = 0.9$ ns. The Coulomb interaction $u_{CaCa}^{Coulomb}(r; \epsilon_r = 71)$ (dashed curve) and the Coulomb plus polarization deficiency interactions $u_{CaCa}^{Coulomb}(r; \epsilon_r = 71) + u_{CaCa}^{pol}(r)$ with $\delta_{Ca} = 23$ M^{-1} and $\delta_{Cl} = 2$ M^{-1} (dotted curve) are also shown. The simulated data were vertically adjusted to agree with dotted curve at $r = 10$ Å.

Figure 9 shows the short-range part of the effective $Me^{2+}-Me^{2+}$, $Me^{2+} = (Mg^{2+}, Ca^{2+}, Sr^{2+}, Ba^{2+})$ potentials. The short-range parts of the effective $Me^{2+}-Cl^-$ potentials are presented in Figure 10. First, we notice that, as for the $Ca^{2+}-Ca^{2+}$ pair, the other effective $Me^{2+}-Me^{2+}$ potentials have a remaining tail, demonstrating that the potential is not yet Coulombic at $r = 10$ Å, whereas no such tail appears for the $Me^{2+}-Cl^-$ potentials. The only exception from the asymptote $u_{MeMe}^{pol}(r)$ between r = 8 and 10 Å is observed for one of the two strontium−strontium potentials. This might be an artifact, as the uncertainty of the simulated potentials can reach 0.1 *kT*. The closest minimum of a $Me^{2+}-Me^{2+}$ potential appears at ≈7 Å, implying solvent-separated structures. Moreover, the minima for the different alkaline earth ions are similar (Figure 9) despite the differences in their size, suggesting that the strength of the water ordering in the first hydration shells partly compensates the effect of the ionic size. The short-range $Me^{2+}-Cl^-$ potentials display a

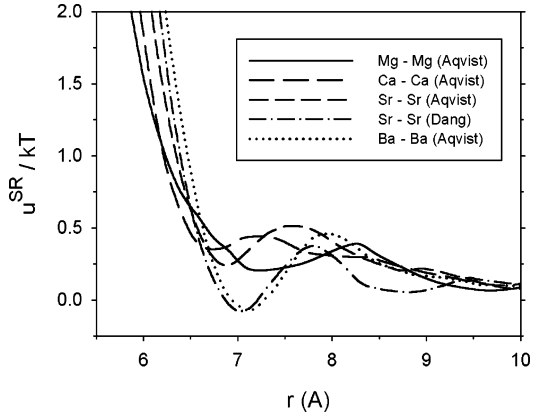

Figure 9. Short-range parts of effective alkaline earth ion−alkaline earth ion potentials from MD simulations by using SPC/E water with Mg^{2+} (solid curve), Ca^{2+} (long-dashed curve), Sr^{2+} (short-dashed curve), and Ba^{2+} (dotted curve) LJ parameters from ref 6 and Sr^{2+} (dash−dotted curve) LJ parameters from ref 10. $t_{MD} = 1.8$ ns ($Ca^{2+}-Ca^{2+}$) and 0.9 ns (other potentials).

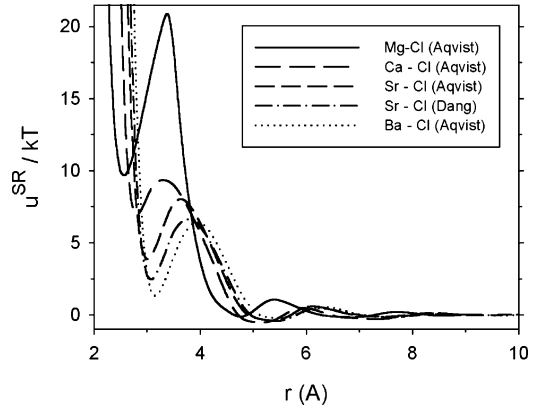

Figure 10. Short-range parts of effective alkaline earth ion−chloride ion potentials from MD simulations by using SPC/E water and Cl^- LJ parameters from ref 8. Notation according to Figure 9. $t_{MD} = 1.8$ ns ($Ca^{2+}-Cl^-$) and 0.9 ns (other potentials).

regular variation at increasing size of Me^{2+} (Figure 10). The location of the close-contact minimum decreases and its magnitude increases with decreasing ionic size.

Mean Ion Activity Coefficients. The effective potentials $u_{ij}(r)$ given by eq 5 were used in solvent-averaged MC simulations to determine mean ion activity coefficients of aqueous $MgCl_2$, $CaCl_2$, $SrCl_2$, and $BaCl_2$ solutions at concentrations between 0.1 and 1 M.

The data in Figures 8−9 showed that contributions from polarization deficiency of the ion hydration shells were significant for the effective $Me^{2+}-Me^{2+}$ potential. An investigation of the role of (i) a permittivity being salt concentration dependent and (ii) the polarization deficiency contributions at $r > r_{max}$ was made. Here, we considered the four cases: (A) $\epsilon_r = \epsilon_{water}$ and $u_{ij}^{pol}(r) = 0$; (B) $\epsilon_r = \epsilon_{water}$ and $u_{ij}^{pol}(r) \neq 0$; (C) $\epsilon_r = \epsilon_{solution}(c)$ and $u_{ij}^{pol}(r) = 0$; and (D) $\epsilon_r = \epsilon_{solution}(c)$ and $u_{ij}^{pol}(r) \neq 0$ for all electrolytes examined.

Experimental ion activity coefficients and simulated ones are shown in Figure 11 (cases A and B) and Figure 12 (cases C and D). Additional atomistic simulations of effective $Ca^{2+}-Ca^{2+}$ and $Ca^{2+}-Cl^-$ potentials suggest error bars in ln $\gamma_\pm$ of $\approx\pm0.05$ at $c = 0.1$ M and $\approx\pm0.2$ at $c = 1$ M. First, the simulations gave the order $\gamma_{CaCl} < \gamma_{BaCl} \approx \gamma_{SrCl} \approx \gamma_{MgCl}$, which is at variant with the experimental order $\gamma_{BaCl} < \gamma_{SrCl} < \gamma_{CaCl} < \gamma_{MgCl}$. Hence, γ_{CaCl} was predicted too low as compared to γ_{BaCl} and γ_{SrCl}, and we were not able to resolve the differences

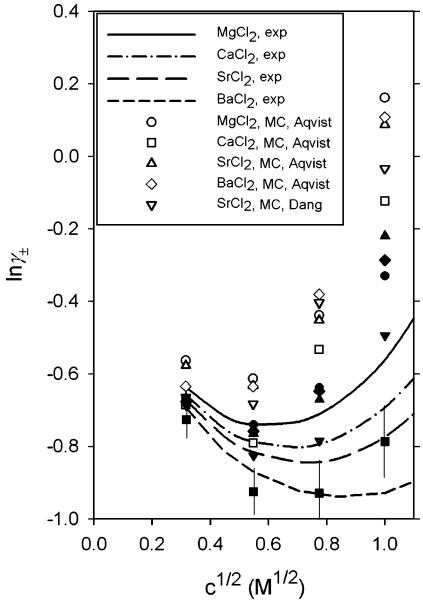

Figure 11. Mean ion activity coefficients vs salt concentration for aqueous solutions of alkaline earth metal chlorides from experiments (curves) and MC simulations (symbols). Notation: $MgCl_2$ (solid curve and circles), $CaCl_2$ (dashed−dotted curve and squares), $SrCl_2$ (long-dashed curve, triangles (Sr^{2+} LJ potential from ref 6) and nablas (Sr^{2+} LJ potential from ref 10)), and $BaCl_2$ (short-dashed curve and diamonds). Equation 5 with $\epsilon_r = \epsilon_{water}$ and $u_{ij}^{pol}(r) = 0$ (filled symbols) or $u_{ij}^{pol}(r) \neq 0$ (open symbols) was used to obtain the effective ion−ion potentials. MC simulation error bars (three standard deviations) are shown for $CaCl_2$ and they are representative for the other electrolytes.

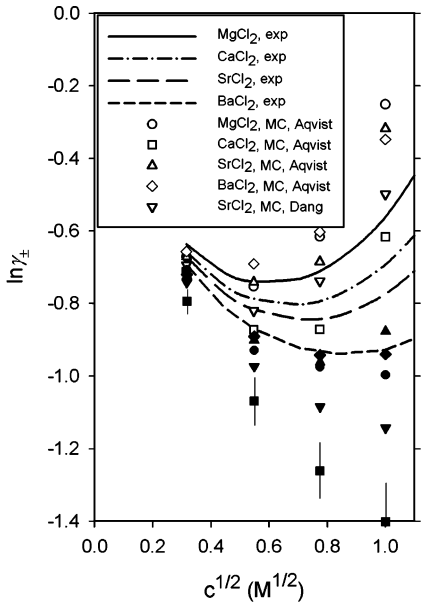

Figure 12. As Figure 11, but with $\epsilon_r = \epsilon_{solution}(c)$.

among γ_{BaCl}, γ_{SrCl}, and γ_{MgCl} despite our lengthy simulations. Small differences in the short-range potential may have large consequences on $\gamma_\pm$, and dissimilar potentials may give similar $\gamma_\pm$. For example, γ_{SrCl} for the two Sr^{2+} models (i) differ widely at $c = 1$ M and (ii) bracket γ_{BaCl} and γ_{MgCl}, despite the similar LJ parameters of the two Sr^{2+} models and the LJ parameters of Mg^{2+} and Ba^{2+} being mutually different and differing with respect to those of Sr^{2+}.

At the lowest salt concentration $c = 0.1$ M, (i) the predicted ion activity coefficients are close to the experimental ones, and (ii) only a limited deviation appears among the four cases. In case A (Figure 11, filled symbols), at higher salt concentrations,

some deviation is observed; all predicted ion activities appear to be higher than the true ones except for $CaCl_2$. If an account for the reduced permittivity at increasing salt concentration as in case C (Figure 12, filled symbols) is taken, the previous overestimation is replaced by an underestimation.

The role of the polarization deficiency term $u_{ij}^{\mathrm{pol}}(r)$ can be seen by comparing results pertaining cases C and D (Figure 12, filled and open symbols). The inclusion of the polarization deficiency term, which makes the effective ion−ion potential more repulsive, raises the ion activity coefficient, and the increase in $\ln \gamma_{\pm}$ grows with increasing salt concentration. The results in Figure 12 without and with polarization deficiency included bracket the experimental ones, which support our notion that the treatment of the polarization deficiency potential as pairwise additive overestimates its contribution.

We assume that eq 6 reasonably well describes the long-range change of the dielectric response at increasing salt concentration. As to the polarization deficiency potential, we will calculate the effect of its truncation at $r = 40$ Å and estimate its contribution if considering it as screened. For simplicity, we consider only the leading contribution arising from the interaction among the divalent cations.

According to expression of the activity coefficients via pair potentials[44] and the expression of $u_{ij}^{\mathrm{pol}}(r)$ given by eq 9, the contribution to the activity coefficient from the interval $R_1 < r < R_2$ from the interaction among species i amounts to

$$\Delta \ln \gamma = \frac{n_i}{kT} \int_{R_1}^{R_2} \mathrm{d}r 4\pi r^2 \int_0^1 \mathrm{d}\lambda (1 + 2\lambda) \alpha_i \left(\frac{q_i}{4\pi\epsilon_0 \epsilon_r r^2} \right)^2 g_{ii}(r, \lambda) \tag{10}$$

where n_i is the number density of species i, q_i the charge of species i (here $q_i = 2e$), λ a coupling parameter, and $g_{ii}(r,\lambda)$ the radial distribution function at the coupling λ. By taking into account that $g_{ii}(r) \approx 1$ for the interval examined and using eq 8, we obtain

$$\Delta \ln \gamma \approx \frac{(2e)^2}{4\pi\epsilon_0 \epsilon_r^2 kT} \delta_i c \left(\frac{1}{R_1} - \frac{1}{R_2} \right) \tag{11}$$

where c is the 2:1 electrolyte concentration, and δ_i the ionic specific factor ($\delta_i = 23$ M^{-1} will be used in the following). First, the truncation of $u_{ij}^{\mathrm{pol}}(r)$ at 40 Å implies an underestimate of $\ln \gamma$ by ≈0.2 at $c = 1$ M. Second, if we, admitting in an ad hoc way, map the overestimation of the polarization deficiency contribution from the treatment as pairwise additive by a truncation to, say, $R = 20$ Å, our predictions in Figure 12 (open symbol) should be reduced ≈0.2 at $c = 1$ M and 0.02 at $c = 0.1$ M. Such a correction would bring the predicted $\gamma_{\pm}$ closer to and in a reasonable agreement with the experimental ones.

Discussion and Conclusions

Ion Hydration and Effective Ion Sizes. We have used several LJ models of alkali and alkaline earth metal cations, a single LJ model of the chloride anion, and the SPC/E water model to simulate effective ion−ion potentials at infinite dilution. Regarding alkali metal ions, we have employed potentials by Åqvist and by Dang, whereas for alkaline earth metal cations, we mainly used potentials by Åqvist. The potentials by Åqvist were constructed by fitting to experimental free energies of ion hydration, whereas those by Dang were constructed by fitting to gas-phase binding enthalpy data.

The primitive model is frequently used to describe electrolyte solutions. In this model, charged hard spheres represent the simple ions and the solvent enters by its permittivity. The ionic diameters are assumed to be pairwise additive. Our simulated effective short-range ion−ion potentials can be used (i) to estimate the ion−ion hard-core distances and (ii) to assess the pairwise additivity assumption. The separation, at which $u^{\mathrm{SR}}(r) \approx 2-3\ kT$ for like-charge ions and $u(r) \approx 2-3\ kT$ for opposite-charge ions, will be taken as a measure of the hard-core ion diameter.

TABLE 3: Estimated Hard-Core Diameters of Hydrated Ions[a]

Me	d_{MeMe} (Å)	d_{MeCl} (Å)	$(d_{\mathrm{MeMe}} + d_{\mathrm{ClCl}})/2$ (Å)[b]
Li^+	3.8 (*)	3.3(*)[c]	4.2
Na^+	3.2	2.7	3.9
K^+	3.6	2.9	4.1
Mg^{2+}	5.9 (*)	3.8 (*)	5.2
Ca^{2+}	6.0 (*)	3.9 (*)	5.3
Sr^{2+}	6.1 (*)	4.0 (*)[c]	5.3
Ba^{2+}	6.3 (*)	4.1 (*)[c]	5.4

[a] d_{ij} denotes the separation at which $u_{ij}^{\mathrm{SR}}(r)$ and $u_{ij}(r)$ attain $2-3\ kT$ for interactions of like-charge ions and of opposite-charge ions, respectively. The asterisk denotes a solvent-separated ion-pair. [b] $d_{\mathrm{ClCl}} = 4.5$ Å. [c] A thermally relevant close-contact ion-pair appearing at ≈1.5 Å shorter separation exists.

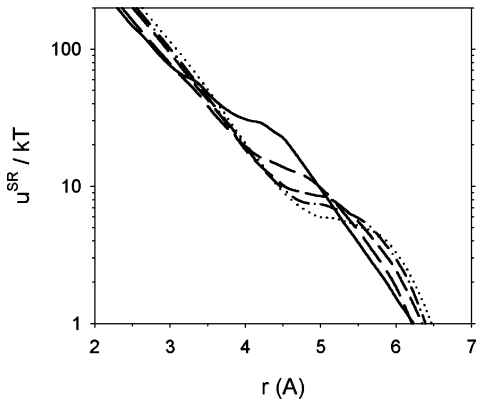

Figure 13. Short-range parts of effective alkaline earth ion−alkaline earth ion potentials in a lin-log scale. Conditions and notation as in Figure 9.

As to the $Cl^- - Cl^-$ potential, Figure 4 suggests the hard-core diameter $d_{\mathrm{ClCl}} \approx 4.5$ Å. At the separation $r = d_{\mathrm{ClCl}}$, two chloride ions are in close contact. In Table 3, we summarize d_{MeMe} as extracted from Figures 4 and 9 and d_{MeCl} from Figures 5 and 10. Regarding Me−Cl^- pairs involving Na^+ or K^+, the hard-core diameters correspond to close-contact ion-pairs. The other cases involve solvent-separated ion-pairs, where sometimes close-contact ion-pairs are present with only a few kT higher free energy than the solvent-separated minimum (Li^+−Cl^-, Sr^{2+}−Cl^-, and Ba^{2+}−Cl^-). Finally, Table 3 also provides the mixed cation−anion diameter as obtained from the pairwise assumption $(d_{\mathrm{MeMe}} + d_{\mathrm{ClCl}})/2$.

The hard-core diameters of the alkaline earth metal ions are about 6 Å. Counterions of such size may cause pronounced overneutralization effects in the vicinity of highly charged polyelectrolytes due to the 6 Å ionic diameter.[45] The origin of the comparable large effective size is the high energy of removing water molecules in the first ionic hydration shell. Despite the fact that accurate calculation of such energies evidently requires a polarizable water model, one can conclude from using the SPC/E water model that such energy can reach tens of kT. Figure 13 shows $u_{ii}^{\mathrm{SR}}(r)$, displayed in Figure 9, in a different scale. The energy of the water removal for the Me^{2+}−Me^{2+} pairs is estimated from the inflection points of curves

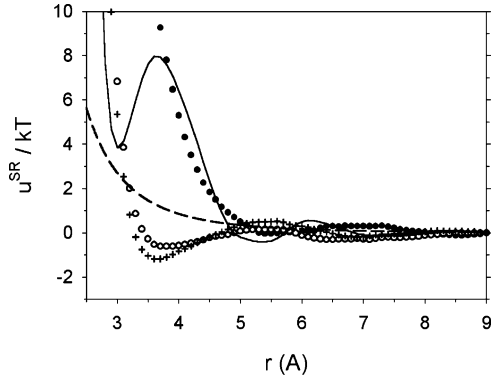

Figure 14. Short-range part of the effective $Sr^{2+}-Cl^-$ potential $u^{SR}(r)$ (from Figure 10, Sr^{2+} LJ potential from ref 10) as well as PMF's obtained with uncharged chloride ion (filled circles), uncharged strontium ion (open circles), and uncharged strontium and chloride ions (crosses) obtained by MD simulations by using a spherical cavity according to Figure 1. $t_{MD} = 0.1$ ns. The polarization deficiency term $\alpha_{Sr}E^2_{Cl}(r) + \alpha_{Cl}E^2_{Sr}(r)$, evaluated with $\delta_{Sr} = 22\ M^{-1}$ and $\delta_{Cl} = 2\ M^{-1}$, is also shown (dashed curve).

and follows the expected sequence Mg^{2+}, Ca^{2+}, Sr^{2+}, and Ba^{2+}, where the highest energy is required for Mg^{2+}. Moreover, our results show that the hydration shell is retained for the smallest alkaline earth metal ions in the $Me^{2+}-Cl^-$ pairs. For $Sr^{2+}-Cl^-$, the free energies of the close-contact and solvent-separated minima are similar (Figure 7).

Further insight in the origin of the short-range effective potentials can be obtained from simulations where the charge of one or both ions is removed. Figure 14 displays the short-range part of the effective $Sr^{2+}-Cl^-$ potential and the corresponding PMFs with either Sr^{2+}, Cl^-, or both ions being uncharged. It is clear that the charge of the divalent cation is essential for the solvent-related repulsion appearing at 3−5 Å separation between the ions, whereas the charge of the chloride ion has only a marginal influence. Similar observation was obtained for monovalent cations (data not shown). This difference reflects the unequal strength of the hydration of cations and anions, even when both are monovalent. Moreover, Figures 5 and 10 unambiguously demonstrate that the solvent-related repulsion, appearing as the solvent-separated state is transferred into the close-contact state, increases with decreasing cation size. This confirms the stronger hydration appearing for small cations, as for example illustrated by the distributions of water molecules near ions (see, e.g., refs 46 and 47).

The discrete nature of the solvent gives rise to an oscillatory PMF at short separation (<8 Å) and a systematic deviation from the dielectrically screened Coulomb interaction at short and intermediate ion−ion separations. Both effects are included in our $u_{ij}^{SR}(r)$. The former effect is due to the interference of the hydration shells of the two ions and the latter one due to the ordering of water molecules in the hydration shells. Figure 14 shows how the oscillatory behavior of $u_{ij}^{SR}(r)$ decays at increasing separation and approaches $u_{ij}^{pol}(r)$ (as calculated according to eqs 8 and 9), representing the polarization deficiency term. A dielectric description is in principle incapable of catching the oscillation behavior of the PMF between like-charged ions.[48]

Initially, neglecting the complication with close-contact minima with higher free energy, we found the pairwise assumption being violated in all cases [$(d_{MeMe} + d_{ClCl})/2 \approx d_{MeCl} + 1$ Å]. This implies that the ions appear smaller in the unlike-pair as compared to the like-pair. Because most thermodynamic quantities in the primitive model are quite sensitive to the hard-core potentials,[49] it seems that at least three independent parameters of ion−ion hard-core interactions should be incorporated into an approximate dielectric theory of electrolytes.

Mean Ion Activity Coefficients. The effective ion−ion potentials were employed to simulate mean ion activity coefficients of electrolytes employing an implicit-solvent description. When assessing the usefulness of the different cationic models against experimental data, it should be noted that this assessment is conditional, as we use the SPC/E water model and a given chloride ion model. The relative merits of the different cationic models could be different with other water and/or chloride ion models.

Monovalent Cations. For alkali metal ions, the most successful prediction was obtained for NaCl solutions. Both Dang's[9] and Åqvist's[6] Na^+ models, with considerable different LJ parameters, produced similar effective ion−ion potentials (Figures 4 and 5), leading to a good agreement between simulated and experimental γ_{NaCl} (Figure 6). As to potassium cation, the results of Dang's[9] K^+ model is acceptable, whereas the predicted γ_{KCl} by Aqvist's[6] K^+ model is apparently incorrect (Figure 6) despite the fact that this model is of equivalent quality to reproduce the free energy of ion hydration.[6] The Li^+ models by Dang[11] and Åqvist[6] lead to underestimation of γ_{LiCl}, but the results are still qualitatively correct (Figure 6). The correct order $\gamma_{KCl} < \gamma_{NaCl} < \gamma_{LiCl}$ was reproduced.

With monovalent ions, the straightforward use of short-range effective ion−ion obtained at infinite dilution augmented by a Coulomb term is capable to describe experimental $\gamma_\pm$, even at high salt concentration. In this aspect, our results confirm those of Lyubartsev and Laaksonen.[16]

Finally, the LJ parameters of Dang's[9] and Åqvist's[6] Na^+ models differ considerably with respect to each other (see Table 2). Thus, if only one experimental property is used to determine the LJ parameters, the determined LJ parameters become not necessarily unique. Hence, LJ parameters should ideally be optimized with respect to several independent experimental properties to narrow down the ambiguity in the assessment of their values.

Divalent Cations. We found that activity coefficients with alkaline earth metal ions are well predicted at $c = 0.1$ M. At this concentration, the differences in γ_{MeCl} among the cations are small, suggesting that the bare Coulomb interaction is dominating.

The prediction of γ_{MeCl} at higher salt concentration possesses several challenges, originating from the vital consequences of the strong ion−water interactions. To improve such a prediction, we have introduced in our analysis (i) a solution permittivity being dependent on the salt concentration and (ii) a potential term representing the dielectric saturation of water molecules near divalent cations. The former extension is based on experimental observations that the permittivity of an aqueous salt solution decreases with increasing salt concentration. A lower permittivity reduces $\gamma_\pm$ because the reduced dielectric screening of the solution increases the magnitude of all Coulomb interactions. The polarization deficiency term originates from the reduced dielectric response of the water molecules in the hydration shell of, in particular, the divalent cations. As a consequence, the effective cation−cation potential becomes more repulsive, leading to an increase in $\gamma_\pm$. Our study shows that these two effects becomes progressively more important at increasing c, $c > 0.1$ M. With the relation $\epsilon_r = \epsilon_{solution}(c)$ taken from experiments from high-frequency impedances for bulk electrolytes and the more ad hoc inclusion of the polariza-

tion deficiency contribution, we found it possible to reproduce experimental mean ion activity coefficients.

Nevertheless, the situation is, however, still not satisfactory. We were not yet able to predict a correct trend among the alkaline earth metal ions, and the strong magnification of the statistical uncertainties of the effective ion−ion potentials onto the mean ion activity coefficients is still troublesome.

Acknowledgment. Financial support from the Swedish Research Council (VR) and computation resources of the Moscow Joint Supercomputer Center (JSCC) are gratefully acknowledged.

References and Notes

(1) Berendsen, H. J. C.; Postma, J. P. M.; van Gunsteren, W. F.; Hermans, J. In *Intermolecular Forces*; Pullman, B., Ed.; Reidel: Dordrecht, The Netherlands, 1981; pp 331−342.
(2) Berendsen, H. J. C.; Grigera, J. R.; Straatsma, T. P. *J. Phys. Chem*. **1987**, *91*, 6269.
(3) Chandrasekhar, J.; Spellmeyer, D. C.; Jorgensen, W. L. *J. Am. Chem. Soc.* **1984**, *106*, 903.
(4) Jorgensen, W. L.; Chandrasekhar, J.; Madura, J. D.; Impey, R. W.; Klein, M. L. *J. Chem. Phys*. **1983**, *79*, 926.
(5) Caldwell, J.; Dang, L. X.; Kollman, P. A. *J. Am. Chem. Soc*. **1990**, *112*, 9144.
(6) Åqvist, J. *J. Phys. Chem.* **1990**, *94*, 8021.
(7) Straatsma, T. P.; Berendsen, H. J. *J. Chem. Phys.* **1988**, *89*, 5876.
(8) Smith, D. E.; Dang, L. X. *J. Chem. Phys.* **1994**, *100*, 3757.
(9) Dang, L. X. *J. Am. Chem. Soc.* **1995**, *117*, 6954.
(10) Smith, D. E.; Dang, L. X. *Chem. Phys. Lett.* **1994**, *230*, 209.
(11) Dang, L. X. *J. Chem. Phys*. **1992**, *96*, 6970.
(12) (a) Patey, G. N.; Carnie, S. L. *J. Chem. Phys.* **1983**, *78*, 5183. (b) Kusalik, P. G.; Patey, G. N. *J. Chem. Phys.* **1988**, *88*, 7715. (c) Kusalik, P. G.; Patey, G. N. *J. Chem. Phys.* **1988**, *89*, 5843. (d) Kusalik, P. G.; Patey, G. N. *J. Chem. Phys.* **1988**, *89*, 7478.
(13) Lyubartsev, A. P.; Laaksonen, A. *J. Phys. Chem*. **1996**, *100*, 16410.
(14) Hummer, G.; Soumpasis, D. M.; Neumann, M. *Mol. Phys*. **1993**, *81*, 1155.
(15) Lyubartsev, A. P.; Laaksonen, A. *Phys. Rev. E* **1995**, *52*, 3730.
(16) Lyubartsev, A. P.; Laaksonen, A. *Phys. Rev. E* **1997**, *55*, 5689.
(17) Lyubartsev, A. P.; Laaksonen, A. *J. Chem. Phys*. **1999**, *111*, 11207.
(18) Pettitt, B. M.; Rossky, P. J. *J. Chem. Phys*. **1986**, *84*, 5836.
(19) Dang, L. X.; Smith, D. E. *J. Chem. Phys.* **1995**, *102*, 3483.
(20) Perera, L.; Essmann, U.; Berkowitz, M. L. *J. Chem. Phys.* **1995**, *102*, 450.
(21) Guardia, E.; Robinson, A.; Padro, J. A. *J. Chem. Phys*. **1993**, *99*, 4229.
(22) Dang, L. X.; Pettitt, B. M.; Rossky, P. J. *J. Chem. Phys*. **1992**, *96*, 4046.
(23) Guardia, E.; Rey, R.; Padro, J. A. *J. Chem. Phys*. **1991**, *95*, 2823.
(24) Ramanathan, P. S.; Friedman, H. L. *J. Chem. Phys*. **1971**, *54*, 1086.
(25) Prigogine, I.; Mazur, P.; Defay, R. *J. Chim. Phys.* **1953**, *50*, 146.
(26) Bolt, G. H. *J. Colloid Sci.* **1955**, *10*, 206.
(27) Sparnaay, M. J. *Recl. Trav. Chim. Pays-Bas* **1958**, *77*, 872.
(28) Levine, S.; Wrigley, H. E. *Discuss. Faraday Soc.* **1957**, *24*, 43.
(29) Levine, S.; Rosenthal, D. K. In *Chemical Physics of Ionic Solutions*, Conway, B. E., Barradas, R. G., Eds.; Wiley: New York, 1966.
(30) Linse, P. *J. Phys. Chem*. **1986**, *90*, 6821.
(31) Gavryushov, S.; Linse, P. *J. Phys. Chem. B* **2003**, *107*, 7135.
(32) Svishchev, I. M.; Kusalik, P. G. *J. Phys. Chem*. **1994**, *98*, 728.
(33) Berendsen, H. J. C.; Postma, J. P. M.; van Gunsteren, W. F.; DiNola, A.; Haak, J. R. *J. Chem. Phys*. **1984**, *81*, 3684.
(34) Linse, P. *MOLSIM*, version 3.0; Lund University: Lund, Sweden, 2000.
(35) Hasted, J. B.; Ritson, D. M.; Collie, C. H. *J. Chem. Phys*. **1948**, *16*, 1.
(36) Harris, F. E.; O'Konski, C. T. *J Phys. Chem*. **1957**, *61*, 310.
(37) There are no reported experimental data for strontium. Here, $\delta_{Sr} = 22\ M^{-1}$ has been used, which is between $\delta_{Ca} \approx 23-24\ M^{-1}$ and $\delta_{Ba} \approx 20\ M^{-1}$.
(38) Karlström, G. *J. Phys. Chem. B* **2002**, *106*, 5302.
(39) Hribar, B.; Southall, N. T.; Vlachy, V.; Dill, K. A. *J. Am. Chem. Soc*. **2002**, *124*, 12302.
(40) Widom, B. *J. Chem. Phys*. **1963**, *39*, 2808.
(41) Svensson, B. R.; Woodward, C. E. *Mol. Phys*. **1988**, *64*, 247.
(42) Stokes, R. H.; Robinson, R. A. *J. Am. Chem. Soc*. **1948**, *70*, 1870.
(43) Toukan, K.; Rahman, A. *Phys. Rev. B* **1985**, *31*, 2643.
(44) Hill, T. L. In *Statistical Mechanics*; McGeaw-Hill: New York, 1956.
(45) Gavryushov, S.; Zielenkiewicz, P. *Biophys. J.* **1998**, *75*, 2732.
(46) Lee, S. H.; Rasaiah, J. C. *J. Phys. Chem*. **1996**, *100*, 1420.
(47) Babu, C. S.; Lim, C. *J. Phys. Chem. B* **1999**, *103*, 7958.
(48) Rashin, A. A. *J. Phys. Chem*. **1989**, *93*, 4664.
(49) Sloth, P.; Sorensen, T. S. *J. Phys. Chem*. **1990**, *94*, 2116.